

Adversarial Image Generation and Training for Deep Neural Networks

Hai Shu,¹ Ronghua Shi,² Hongtu Zhu,³ Ziqi Chen⁴

¹ Department of Biostatistics, New York University, New York, USA

² School of Mathematics and Statistics, Central South University, Changsha, China

³ AI Labs, Didi Chuxing, Beijing, China

zhuhongtu@didiglobal.com

⁴ Key Laboratory of Advanced Theory and Application in Statistics and Data Science-MOE,
School of Statistics, East China Normal University, Shanghai, China

zqchen@fem.ecnu.edu.cn

Abstract

Deep neural networks (DNNs) have achieved great success in image classification, but they may be very vulnerable to adversarial attacks with small perturbations to images. Moreover, the adversarial training based on adversarial image samples has been shown to improve the robustness and generalization of DNNs. The aim of this paper is to develop a novel framework based on information-geometry sensitivity analysis and the particle swarm optimization to improve two aspects of adversarial image generation and training for DNNs. The first one is customized generation of adversarial examples. It can design adversarial attacks from options of the number of perturbed pixels, the misclassification probability, and the targeted incorrect class, and hence it is more flexible and effective to locate vulnerable pixels and also enjoys certain adversarial universality. The other is targeted adversarial training. DNN models can be improved in training with the adversarial information using a manifold-based influence measure effective in vulnerable image/pixel detection as well as allowing for targeted attacks, thereby exhibiting an enhanced adversarial defense in testing.

1 Introduction

Deep neural networks (DNNs) have exhibited exceptional performance in image classification (Krizhevsky, Sutskever, and Hinton 2012; He et al. 2016; Huang et al. 2017) and thus are widely used in various real-world applications including face recognition (Sun et al. 2015), self-driving cars (Bojarski et al. 2016), biomedical image processing (Bakas et al. 2018), among many others (Najafabadi et al. 2015). Despite these successes, DNN classifiers can be easily attacked by adversarial examples with perturbations imperceptible to human vision (Szegedy et al. 2013; Goodfellow, Shlens, and Szegedy 2014; Su, Vargas, and Sakurai 2019). This motivates the hot research in adversarial attacks and defenses of DNNs. See Wiyatno et al. (2019) and Ren et al. (2020) for reviews.

Existing adversarial attacks can be categorized into white-box, gray-box, and black-box attacks. Adversaries in white-box attacks have the full information of their targeted DNN model, whereas their knowledge is limited to model structure in gray-box attacks and only to model's input and output in black-box attacks. For instance, popular algorithms for white-box attacks include the fast gradient sign method (Goodfellow, Shlens, and Szegedy 2014; Kurakin, Goodfellow, and

Bengio 2016), the projected gradient descent method (Madry et al. 2017), the Carlini and Wagner attack (Carlini and Wagner 2017), among many others (Szegedy et al. 2013; Papernot et al. 2016; Moosavi-Dezfooli, Fawzi, and Frossard 2016). Defensive techniques for those attacks include heuristic and certificated defenses. Adversarial training is the current most successful heuristic defense approach for improving the robustness of DNNs, which simply incorporates adversarial samples into training but has better numerical performance than certificated defenses (Ren et al. 2020).

In this paper, we propose a simple yet efficient framework for white-box adversarial image generation and training for DNN classifiers. For generating an adversarial example of a given image, our framework provides user-customized options in the number of perturbed pixels, misclassification probability, and targeted incorrect class. To the best of our knowledge, this is the first approach rendering all the three desirable options. The freedom to specify the number of perturbed pixels allows users to conduct attacks at various pixel levels such as one-pixel (Su, Vargas, and Sakurai 2019) and all-pixel (Moosavi-Dezfooli et al. 2017) attacks. Particularly, we adopt a recent perturbation-manifold based first-order influence (FI) measure (Shu and Zhu 2019) to efficiently locate the most vulnerable pixels to increase the attack success rate. In contrast with traditional Euclidean-space based measures such as Jacobian norm (Novak et al. 2018) and Cook's local influence measure (Cook 1986), the FI measure captures the intrinsic change of the perturbed objective function (Zhu et al. 2007; Zhu, Ibrahim, and Tang 2011) and shows better performance in detecting vulnerable images and pixels. Besides, our framework allows users to specify the misclassification probability and/or the targeted incorrect class. The prespecified misclassification probability is rarely seen in existing approaches, which produce an adversarial example either near the model's decision boundary (Moosavi-Dezfooli, Fawzi, and Frossard 2016; Nazemi and Fieguth 2019) or with unguaranteed high confidence (Nguyen, Yosinski, and Clune 2015). We tailor different loss functions accordingly to the three desirable options and their combinations, and apply the particle swarm optimization (PSO) (Kennedy and Eberhart 1995), a fast gradient-free method, to obtain the optimal perturbation. Moreover, we observe that our perturbations with high misclassification probability can have certain adversarial universality (Moosavi-Dezfooli et al. 2017) to images from

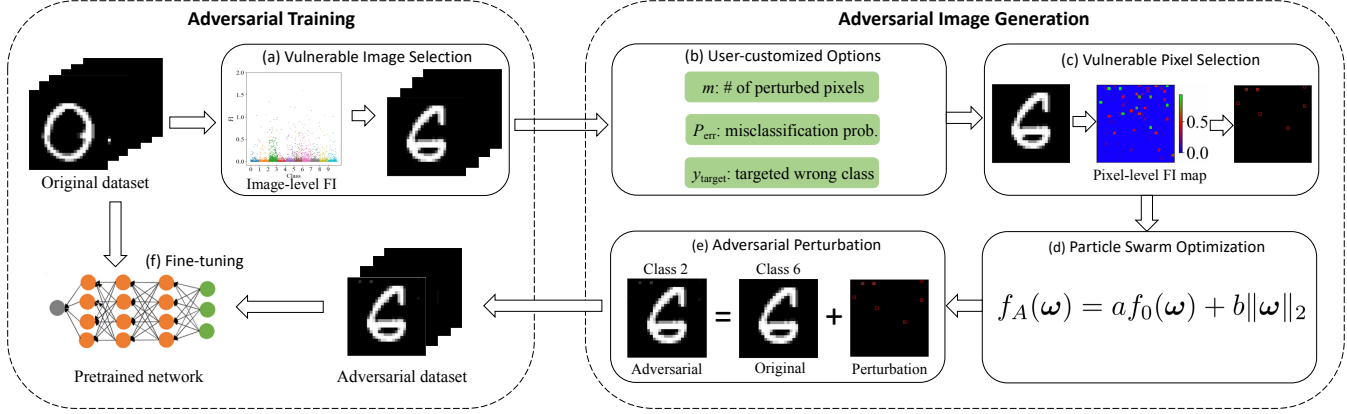


Figure 1: Flowchart of our proposed framework.

different classes. For adversarial training, in training data we further utilize the FI measure to identify vulnerable images and their pixels that are prone to optional targeted classes. Then using our customized generation approach yields an adversarial dataset for training. Experiments show that our adversarial training significantly improves the robustness of pretrained DNN classifiers. Figure 1 illustrates the flowchart of our framework.

We notice that two recent papers (Zhang et al. 2019; Mosli et al. 2019) also applied PSO to craft adversarial images. However, we have intrinsic distinctions. First, the two papers focus on black-box attacks, but ours is white-box. Zhang et al. (2019) only studied all-pixel attacks; although Mosli et al. (2019) considered few-pixel attacks but searched in random chunks to locate the vulnerable pixels, we use the FI measure to directly discover those pixels. Moreover, targeted attacks are not considered in Mosli et al. (2019), and both papers cannot prespecify a misclassification probability for the generated adversarial example. Our framework is able to design arbitrary-pixel-level, confidence-specified, and/or targeted/nontargeted attacks.

Our contributions are summarized as follows:

- We propose a novel white-box framework for adversarial image generation and training for DNN classifiers. It provides users with multiple options in pixel levels, confidence levels, and targeted classes for adversarial attacks and defenses.
- We innovatively adopt a manifold-based FI measure to efficiently identify vulnerable images and pixels for adversarial perturbations.
- We design different loss functions adaptive to user-customized specifications and apply the PSO, a fast gradient-free optimization, to obtain optimal perturbations.
- We demonstrate the effectiveness of our framework via experiments on benchmark datasets and notice that our high-confidence perturbations may have certain adversarial universality.

2 Method

2.1 Perturbation-Manifold Based Influence Measure

Given an input image \mathbf{x} and a DNN classifier N with parameters θ , the prediction probability for class $y \in \{1, \dots, K\}$ is denoted by $P(y|\mathbf{x}, \theta) = N_\theta(y, \mathbf{x})$. Let $\omega = (\omega_1, \dots, \omega_m)^T$ be a perturbation vector in an open set $\Omega \subseteq \mathbb{R}^m$, which can be imposed on any subvector of $(\mathbf{x}^T, \theta^T)^T$. Let the prediction probability under perturbation ω be $P(y|\mathbf{x}, \theta, \omega)$ with $P(y|\mathbf{x}, \theta, \omega_0) = P(y|\mathbf{x}, \theta)$.

For sensitivity analysis of DNNs, Shu and Zhu (2019) recently have proposed an FI measure to delineate the ‘intrinsic’ perturbed change of the objective function on the Riemannian manifold of $\mathcal{M} = \{P(y|\mathbf{x}, \theta, \omega) : \omega \in \Omega\}$ (Zhu et al. 2007; Zhu, Ibrahim, and Tang 2011). In contrast with traditional Euclidean-space based measures such as Jacobian norm (Novak et al. 2018) and Cook’s local influence measure (Cook 1986), this perturbation-manifold based measure enjoys the desirable invariance property under diffeomorphic (e.g., scaling) reparameterizations of perturbations and has better numerical performance in detecting vulnerable images and pixels.

Let $f(\omega)$ be an objective function of interest, for example, the cross-entropy $f(\omega) = -\log P(y = y_{\text{true}}|\mathbf{x}, \theta, \omega)$. The FI measure at $\omega = \omega_0$ is defined by

$$\text{FI}_\omega(\omega_0) = [\partial_\omega f(\omega_0)] \mathbf{G}_\omega^\dagger(\omega_0) [\partial_\omega f(\omega_0)]^T, \quad (1)$$

where $\partial_\omega = (\partial/\partial\omega_1, \dots, \partial/\partial\omega_p)$, $\mathbf{G}_\omega(\omega) = \sum_{k=1}^K \partial_\omega^T \ell(\omega|y, \mathbf{x}, \theta) \partial_\omega \ell(\omega|y, \mathbf{x}, \theta) P(y|\mathbf{x}, \theta, \omega)$ with $\ell(\omega|y, \mathbf{x}, \theta) = \log P(y|\mathbf{x}, \theta, \omega)$, and $\mathbf{G}_\omega^\dagger(\omega_0)$ is the pseudoinverse of $\mathbf{G}_\omega(\omega_0)$. A larger value of $\text{FI}_\omega(\omega_0)$ indicates that the DNN model is more sensitive in $f(\omega)$ to local perturbation ω around ω_0 .

We shall apply the FI measure to discover vulnerable images or pixels for adversarial perturbations. It is worth mentioning that Shu and Zhu (2019) did not develop an optimization algorithm for adversarial attacks that incorporates their proposed FI measure. We will connect the FI measure to adversarial attacks by our devised optimizations that can be solved by the PSO algorithm.

2.2 Particle Swarm Optimization

Since introduced by Kennedy and Eberhart (1995), the PSO algorithm has been successfully used in solving complex optimization problems in various fields of engineering and science (Poli 2008; Eberhart and Shi 2001; Zhang, Wang, and Ji 2015). Let f_A be an objective function, which will be specified in Section 2.3 for adversarial scenarios. The PSO algorithm performs searching via a population (called swarm) of candidate solutions (called particles) by iterations to optimize the objective function f_A . Specifically, let

$$\mathbf{p}_{i,\text{best}}^t = \arg \min_{k=1,\dots,t} f_A(\boldsymbol{\omega}_i^k), \quad i \in \{1, 2, \dots, N_p\}, \quad (2)$$

$$\mathbf{g}_{\text{best}}^t = \arg \min_{i=1,\dots,N_p} f_A(\mathbf{p}_{i,\text{best}}^t), \quad (3)$$

where $\boldsymbol{\omega}_i^k = (\omega_{i1}^k, \dots, \omega_{im}^k)^T$ is the position of particle i in an m -dimensional space at iteration k , N_p is the total number of particles, and t is the current iteration. The position, $\boldsymbol{\omega}_i^{t+1}$, of particle i at iteration $(t+1)$ is updated with a velocity $\mathbf{v}_i^{t+1} = (v_{i1}^{t+1}, \dots, v_{im}^{t+1})$ by

$$\begin{aligned} \mathbf{v}_i^{t+1} &= w\mathbf{v}_i^t + c_1 r_1 (\mathbf{p}_{i,\text{best}}^t - \boldsymbol{\omega}_i^t) + c_2 r_2 (\mathbf{g}_{\text{best}}^t - \boldsymbol{\omega}_i^t), \\ \boldsymbol{\omega}_i^{t+1} &= \boldsymbol{\omega}_i^t + \mathbf{v}_i^{t+1}, \end{aligned} \quad (4)$$

where w is the inertia weight, c_1 and c_2 are acceleration coefficients, and r_1 and r_2 are uniformly distributed random variables in the range $[0, 1]$. Following Xu et al. (2019), we fix $w = 0.6$ and $c_1 = c_2 = 2$. We can see that the movement of each particle is guided by its individual best known position and the entire swarm's best known position. We shall use the PSO algorithm to obtain desirable adversarial perturbations under various user's requirements.

2.3 Adversarial Image Generation

Given an image \mathbf{x} , we innovatively combine FI and PSO to generate its adversarial image with user-customized options for the number of pixels for perturbation, the misclassification probability, and the targeted class to which the image is misclassified, denoted by m , P_{err} , and y_{target} , respectively.

Denote image $\mathbf{x} = (x_1, \dots, x_p)^T$. For an RGB image of q pixels, we view the three channel components of a pixel as three separate pixels, so $p = 3q$ here. We let the default value of $m = p$.

We first locate m vulnerable pixels in \mathbf{x} for perturbation, if m is specified but the targeted pixels are not given by the user. We compute the FI measure in (1) for each pixel $i \in \{1, \dots, p\}$ based on the objective function

$$f(\boldsymbol{\omega}) = \begin{cases} -\log P(y_{\text{true}}|\mathbf{x}, \boldsymbol{\theta}, \boldsymbol{\omega}), & \text{if } y_{\text{target}} \text{ is not given,} \\ -\log P(y_{\text{target}}|\mathbf{x}, \boldsymbol{\theta}, \boldsymbol{\omega}), & \text{otherwise,} \end{cases} \quad (5)$$

where $\boldsymbol{\omega} = \Delta \mathbf{x}_i$. Denote $x_{(i)}$ to be the pixel with the i -th largest FI value. We use $x_{(1)}, \dots, x_{(m)}$ as the m pixels for adversarial attack and let perturbation $\boldsymbol{\omega} = (\omega_1, \dots, \omega_m)^T = (\Delta x_{(1)}, \dots, \Delta x_{(m)})^T$.

We then apply the PSO in (2) and (4) to obtain an optimal value of $\boldsymbol{\omega}$ that minimizes the adversarial objective function

$$f_A(\boldsymbol{\omega}) = a f_0(\boldsymbol{\omega}) + b \|\boldsymbol{\omega}\|_2, \quad \omega_i \in \varepsilon \cdot (0 - x_{(i)}, 1 - x_{(i)}),$$

where we assume $x_i \in [0, 1]$, ε constrains the range of perturbation to guarantee the visual quality of the generated adversarial image compared to the original, $f_0(\boldsymbol{\omega})$ is a misclassification loss function, $\|\boldsymbol{\omega}\|_2$ represents the magnitude of perturbation, and a and b are prespecified weights. To ensure the misleading nature of the generated adversarial sample, $a \gg b$ is set to prioritize $f_0(\boldsymbol{\omega})$ over $\|\boldsymbol{\omega}\|_2$.

We design different $f_0(\boldsymbol{\omega})$ functions to meet different user-customized requirements on $\{m, P_{\text{err}}, y_{\text{target}}\}$. If only m is known, inspired by Meng (2018) and Meng and Chen (2017), we let the misclassification loss function be

$$f_0(\boldsymbol{\omega}) = \begin{cases} |P(y_1|\mathbf{x}, \boldsymbol{\theta}, \boldsymbol{\omega}) - P(y_2|\mathbf{x}, \boldsymbol{\theta}, \boldsymbol{\omega})|, & \text{if } y_1 = y_{\text{true}}, \\ 0, & \text{if } y_1 \neq y_{\text{true}}, \end{cases}$$

where y_k is the label with the k -th largest prediction probability $P(y = y_k|\mathbf{x}, \boldsymbol{\theta}, \boldsymbol{\omega})$ from the trained DNN for the input image \mathbf{x} added with perturbation $\boldsymbol{\omega}$. Since $y_1 \neq y_{\text{true}}$ results in the minimum of $f_0(\boldsymbol{\omega})$, this loss function encourages PSO to yield a valid perturbation. If the $\boldsymbol{\omega}$ -perturbed \mathbf{x} is prespecified with a misclassification probability $P_{\text{err}} \geq 0.5$, we use the misclassification loss function

$$f_0(\boldsymbol{\omega}) = \begin{cases} |P(y_2|\mathbf{x}, \boldsymbol{\theta}, \boldsymbol{\omega}) - P_{\text{err}}|, & \text{if } y_1 = y_{\text{true}}, \\ |P(y_1|\mathbf{x}, \boldsymbol{\theta}, \boldsymbol{\omega}) - P_{\text{err}}|, & \text{if } y_1 \neq y_{\text{true}}. \end{cases}$$

Later in our experiments, we show that high P_{err} is helpful to generate universal adversarial perturbations applicable to images from the other classes. If a targeted class y_{target} is given, we choose the misclassification loss function

$$f_0(\boldsymbol{\omega}) = \begin{cases} |P(y_1|\mathbf{x}, \boldsymbol{\theta}, \boldsymbol{\omega}) - P(y_{\text{target}}|\mathbf{x}, \boldsymbol{\theta}, \boldsymbol{\omega})|, & \text{if } y_1 \neq y_{\text{target}}, \\ 0, & \text{if } y_1 = y_{\text{target}}. \end{cases}$$

Furthermore, if both P_{err} and y_{target} are provided, we use

$$f_0(\boldsymbol{\omega}) = \begin{cases} |P(y_1|\mathbf{x}, \boldsymbol{\theta}, \boldsymbol{\omega}) - P(y_{\text{target}}|\mathbf{x}, \boldsymbol{\theta}, \boldsymbol{\omega})|, & \text{if } y_1 \neq y_{\text{target}}, \\ |P(y_1|\mathbf{x}, \boldsymbol{\theta}, \boldsymbol{\omega}) - P_{\text{err}}|, & \text{if } y_1 = y_{\text{target}}. \end{cases}$$

or equivalently $f_0(\boldsymbol{\omega}) = |P(y_{\text{target}}|\mathbf{x}, \boldsymbol{\theta}, \boldsymbol{\omega}) - P_{\text{err}}|$.

Our procedure for generating a customized adversarial image is illustrated in Figure 1 (b)-(e) and also summarized in Algorithm 1.

2.4 Adversarial Training

We aim to create a set of adversarial images for a given trained DNN model, and then fine-tune the model on the training data augmented with this adversarial dataset. To include as many adversarial images as possible, we do not specify a value to P_{err} in Algorithm 1. Note that Algorithm 1 may not have a feasible solution when given with restrictive parameters such as small ε or small N_p . To efficiently generate a batch of adversarial images, we first select a set of potentially vulnerable images by some modifications to Algorithm 1.

Specifically, given an image dataset $X = \{\mathbf{x}_i\}_{i=1}^n$, thresholds $\{\text{FI}_{\text{img}}, P_{\text{target}}, \text{FI}_{\text{pixel}}\}$ and targeted incorrect labels $\{y_{i,\text{target}}\}_{i=1}^n$ (if not given, $y_{i,\text{target}} = y_{i,2}$ the label with the second largest prediction probability), we first find \tilde{X} , the set of all correctly classified images that have image-level FI (with $\boldsymbol{\omega} = \Delta \mathbf{x}_i$) $\geq \text{FI}_{\text{img}}$ and prediction probability

Algorithm 1 Adversarial image generation

Input: Image and label $\{\mathbf{x}, y_{\text{true}}\}$, number of perturbed pixels m , (optional) indices of perturbed pixels, (optional) misclassification probability P_{err} , (optional) targeted incorrect label y_{target} , hyperparameters $\{N_p, a, b, \varepsilon\}$ in PSO, and maximum iteration number T

- 1: If perturbed pixels are not specified, compute FI by (1) and (5) for all pixels to locate the m pixels for perturbation ω ;
- 2: Initialize N_p particles in PSO with positions $\{\{\mathbf{p}_{i,\text{best}}^0 = \omega_i^0\}_{i=1}^{N_p}, \mathbf{g}_{\text{best}}^0\}$ and velocities $\{\mathbf{v}_i^0\}_{i=1}^{N_p}$;
- 3: **Repeat**
- 4: **for** particle $i = 1, \dots, N_p$ **do**
- 5: Update \mathbf{v}_i^t and ω_i^t by (4);
- 6: Update $\mathbf{p}_{i,\text{best}}^t$ by (2);
- 7: **end for**
- 8: Update $\mathbf{g}_{\text{best}}^t$ by (3);
- 9: **Until** convergence or iteration $t = T$

Output: Adversarial image $(\mathbf{x} + \text{zero-padded } \omega)$, where $\omega = \mathbf{g}_{\text{best}}^t$.

Algorithm 2 Adversarial dataset generation

Input: Image set $X = \{\mathbf{x}_i\}_{i=1}^n$ and labels $\{y_{i,\text{true}}\}_{i=1}^n$, thresholds $\{\text{FI}_{\text{img}}, P_{\text{target}}, \text{FI}_{\text{pixel}}\}$, targeted incorrect labels $\{y_{i,\text{target}}\}_{i=1}^n$, and hyperparameters $\{N_p, a, b, \varepsilon, T\}$ in Algorithm 1

- 1: For each correctly classified $\mathbf{x}_i \in X$, compute the image-level FI (denoted by FI_i) by (1) with $\omega = \Delta \mathbf{x}_i$ and $f(\omega) = -\log P(y = y_{i,\text{true}} | \mathbf{x}_i, \theta, \omega)$;
- 2: Determine $\tilde{X} = \{\mathbf{x}_i \in X : \text{FI}_i \geq \text{FI}_{\text{img}}, P(y_{i,\text{target}} | \mathbf{x}_i, \theta) \geq P_{\text{target}}\}$;
- 3: For each $\mathbf{x}_i \in \tilde{X}$, generate its adversarial image \mathbf{x}_i^a by Algorithm 1 with $m = \#$ of pixels with $\text{FI} \geq \text{FI}_{\text{pixel}}$ and $y_{\text{target}} = y_{i,\text{target}}$.

Output: Adversarial dataset $\tilde{X}^a = \{\mathbf{x}_i^a\}_{i=1}^{|\tilde{X}|}$

$P(y_{i,\text{target}} | \mathbf{x}_i, \theta) \geq P_{\text{target}}$. For each image in set \tilde{X} , we generate its adversarial image by Algorithm 1 in which m is the number of pixels with $\text{FI} \geq \text{FI}_{\text{pixel}}$ and y_{target} is specified to $y_{i,\text{target}}$. These generated adversarial images form an adversarial dataset. The whole procedure of our adversarial training is illustrated in Figure 1 and detailed in Algorithm 2.

3 Experiments

We conduct experiments on the two benchmark datasets MNIST (LeCun, Cortes, and Burges 2010) and CIFAR10 (Krizhevsky 2009) using the ResNet32 model (He et al. 2016). Data augmentation is used, including random horizontal and vertical shifts up to 12.5% of image height and width for both datasets, and additionally random horizontal flip for CIFAR10. We train ResNet32 on MNIST and CIFAR10 for 80 and 200 epochs, respectively. Table 1 shows the prediction accuracy of our trained ResNet32 for the two datasets.

Table 1: Accuracy of original and adversarial trained ResNet32 models

Model	MNIST		CIFAR10	
	Training (n=60k)	Testing (n=10k)	Training (n=50k)	Testing (n=10k)
Original	99.76%	99.25%	98.82%	91.28%
Adversarial	99.68%	99.32%	99.10%	91.32%

3.1 Customized Adversarial Image Generation

We consider two images with easy visual detection and large image-level FI in MNIST and CIFAR10, shown in Figures 2 and 3 with prediction-probability graphs and pixel-level FI maps. The probability bar graphs imply candidate misclassification classes that can be used as y_{target} . The FI maps indicate the vulnerability of each pixel to local perturbation and are useful to locate pixels for attack.

We first evaluate the performance of Algorithm 1 (cf. Figure 1 (b)-(e)) in generating adversarial examples of the two images according to different requirements on m , P_{err} and y_{target} . Figures 4 and 5 show the generated adversarial images with corresponding perturbation maps. Perturbations 1-3 consider the settings with $m = 1, 3$, and 7 , respectively, and with no specifications to P_{err} and y_{target} . For Perturbations 4-6, we only specify $P_{\text{err}} = 0.5, 0.75$, and 0.99 , respectively, assign no value to y_{target} , and tune m being the number of pixels with $\text{FI} > \text{FI}_{\text{pixel}} \in \{0.1, 1\}$ and $N_p \in \{200, 500, 1000\}$ to obtain feasible solutions from PSO. Perturbations 7-9 are pre-specified with $y_{\text{target}} = 0, 2$, and 4 for MNIST, and $0, 4$, and 5 for CIFAR10, respectively, m being the number of pixels with $\text{FI} > 0.1$, and no value for P_{err} . The detailed parameter settings for Algorithm 1 are provided in Supplementary Material. We can see that the generated adversarial images have visually negligible differences from the originals and satisfy the prespecified requirements.

We also investigate the adversarial universality of Perturbation 6 shown in Figures 4 and 5, which have 99% prediction probability to Class 4. Table 2 shows the proportions of original correctly-classified images that are misclassified after added with the perturbations. The MNIST dataset has error rates at least 14.3% for all classes and some up to 100%, with a total rate above 87.5% in both training and testing sets. In particular, a remarkably large proportion of each class are misclassified to Class 4 with a total rate of 62.2% and 64.5% for training and testing sets. Perturbation 6 for CIFAR10 also exhibits a certain extent of adversarial universality with non-targeted total error rates 3.92% and 6.19% and Class-4-targeted total rates 0.92% and 1.32% for training and testing sets, respectively. Figure 6 displays images from the other nine classes that are originally correctly classified with high probability but are misclassified (most with high probability) to Class 4 after added with Perturbation 6. These results indicate that our method may generate a universal adversarial perturbation, which particularly has the potential to misclassify images from different classes to the same specific class. The existence of universal adversarial perturbations may be attributed to the geometric correlations of decision

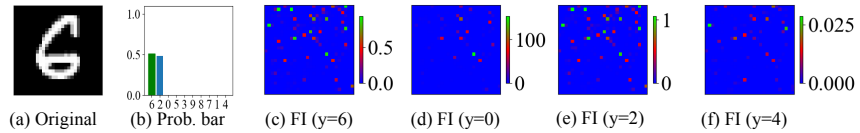


Figure 2: Pixel-level FI maps of an MNIST image for different target classes.

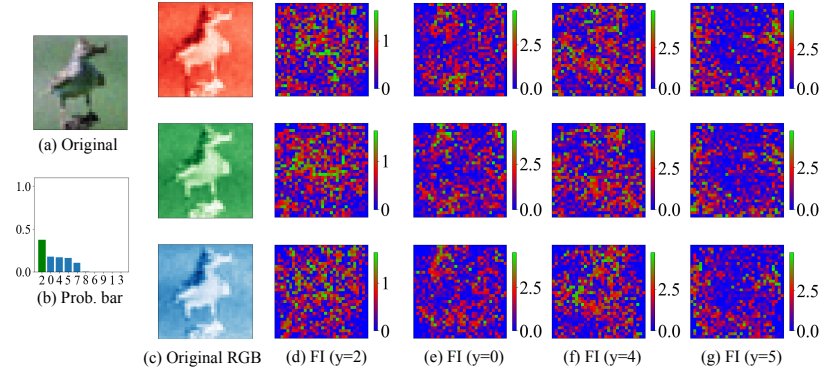


Figure 3: Pixel-level FI maps of a CIFAR10 image's RGB channels for different target classes. Class labels: (0, 1, 2, 3, 4, 5, 6, 7, 8, 9) = (plane, car, bird, cat, deer, dog, frog, horse, ship, truck).

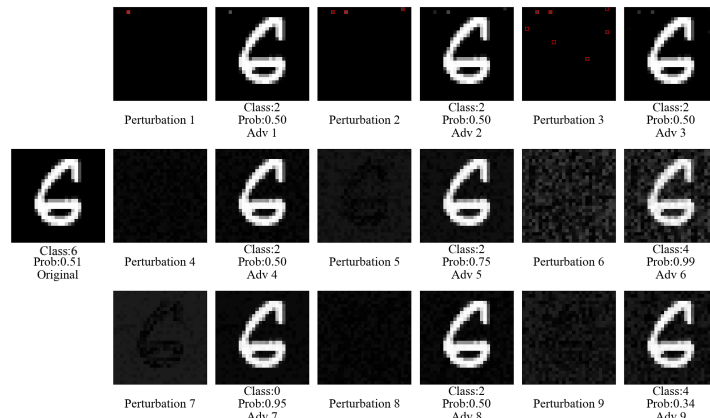


Figure 4: Adversarial examples of an MNIST image. Perturbations 1-3 are set with $m = 1, 3$ and 7 , respectively; Perturbations 4-6 are with $P_{\text{err}} = 0.5, 0.75$ and 0.99 , respectively; Perturbations 7-9 are with $y_{\text{target}} = 0, 2$ and 4 , respectively. Perturbation maps are followed by resulting adversarial images.

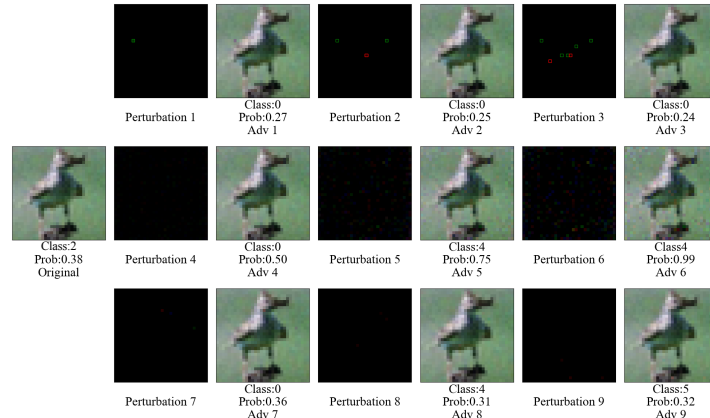


Figure 5: Adversarial examples of a CIFAR10 image. Perturbations 1-3 are set with $m = 1, 3$ and 7 attacked pixels (framed in the attacked channel's color), respectively. Perturbations 4-6 are set with $P_{\text{err}} = 0.5, 0.75$ and 0.99 , respectively. Perturbations 7-9 are set with $y_{\text{target}} = 0, 4$ and 5 , respectively. Perturbation maps are followed by resulting adversarial images.

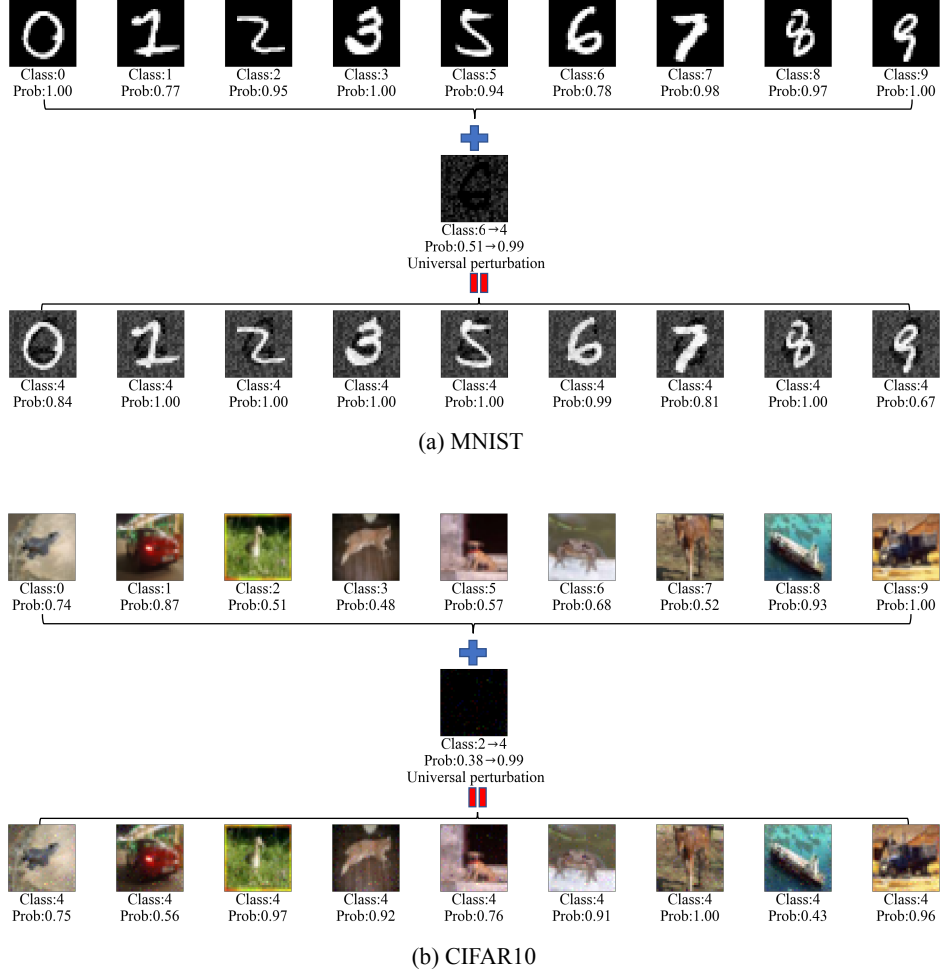


Figure 6: Results of universal adversarial perturbations (Perturbations 6 in Figures 4 and 5).

boundaries between classes (Moosavi-Dezfooli et al. 2017). An adversarial perturbation with very high confidence may have salient features of its resulting class and thus it may have strong power to drag other different images towards the decision boundary.

3.2 Adversarial Training

We consider using Algorithm 2 to generate adversarial datasets for adversarial training. Figure 7 shows the Manhattan plots of image-level FIs for correctly classified images and Figure 8 presents the heatmaps of confusion matrices. We can see that the distributions of image-level FIs and the patterns of misclassifications are very close between training and test datasets in both MNIST and CIFAR10. Our adversarial training is hence expected to be useful for unseen adversarial examples generated from similar mechanisms in testing.

Based on the two figures, for selecting vulnerable images (cf. Figure 1(a)), we let $\text{FI}_{\text{img}} = 0.2$, $y_{i,\text{target}}$ be the most frequent misclassified class of x_i 's true class, and $P_{\text{target}} = 0.2$ in Algorithm 2. The resulting image set \tilde{X} is likely to be near the decision boundaries of the trained classifier. We then

set $\text{FI}_{\text{pixel}} = 0.1$ in the algorithm. We generate adversarial datasets Adv1 ($n = 136$) and Adv2 ($n = 26$), respectively, from training and testing sets of MNIST, and Adv3 ($n = 244$) and Adv4 ($n = 146$) from those of CIFAR10. Adv1 and Adv3 are used for adversarial training (cf. Figure 1(f)), whereas Adv2 and Adv4 test the adversarial trained models. The detailed parameter settings for Algorithm 2 to generate those datasets are given in Supplementary Material.

The adversarial trained ResNet32 models are trained from the original trained models on the training data augmented with Adv1 and Adv3 , respectively, for additional 30 epochs for MNIST and 50 epochs for CIFAR10. The results of adversarial training are reported in Tables 1 and 3. Since the adversarial datasets ($n \leq 244$) are much smaller than original testing datasets ($n = 10k$) and the original trained models already have high accuracy, the results in Tables 1 are only slightly improved on the test datasets. However, in Table 3, the adversarial training on Adv1 and Adv3 indeed benefits the defense of the fine-tuned ResNet32 models against adversarial attacks. The accuracy is dramatically improved from 0.00% to 83.82% and 88.93% on Adv1 and Adv3 , respec-

Table 2: Proportions (in %) of original correctly-classified images that are misclassified after added with Perturbations 6 in Figures 4 and 5.

	True Class	0	1	2	3	5	6	7	8	9	Total
MNIST Training	Misclassified	92.9	100	99.3	91.1	96.0	92.3	100	15.3	99.9	87.7
	Misclass. to 4	81.1	36.9	55.8	84.3	75.5	49.6	95.3	14.2	68.8	62.2
MNIST Testing	Misclassified	91.7	100	99.4	94.4	97.9	91.1	100	14.3	100	87.9
	Misclass. to 4	79.7	37.3	58.8	88.3	78.5	57.4	94.8	13.7	75.0	64.5
CIFAR10 Training	Misclassified	8.46	2.74	2.90	7.27	5.77	0.42	4.82	2.07	1.00	3.92
	Misclass. to 4	1.27	0.04	0.89	1.65	1.45	0.12	2.56	0.30	0.06	0.92
CIFAR10 Testing	Misclassified	11.2	5.62	6.27	12.36	8.29	0.94	6.81	3.05	2.61	6.19
	Misclass. to 4	2.17	0.10	1.48	2.52	2.34	0.31	2.81	0.32	0.21	1.32

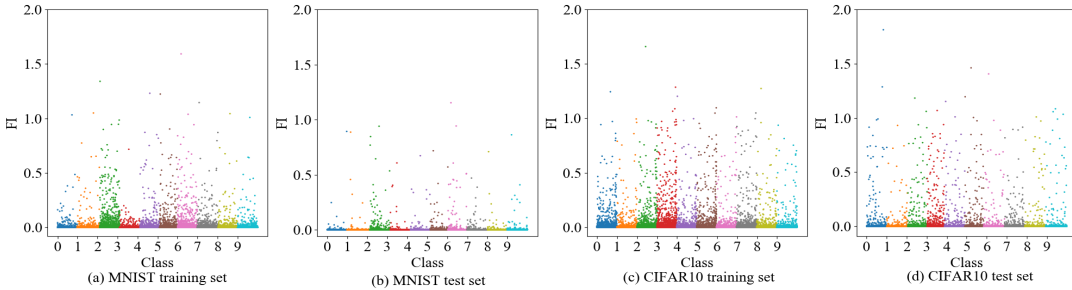


Figure 7: Manhattan plots of image-level FIs for correctly classified images.

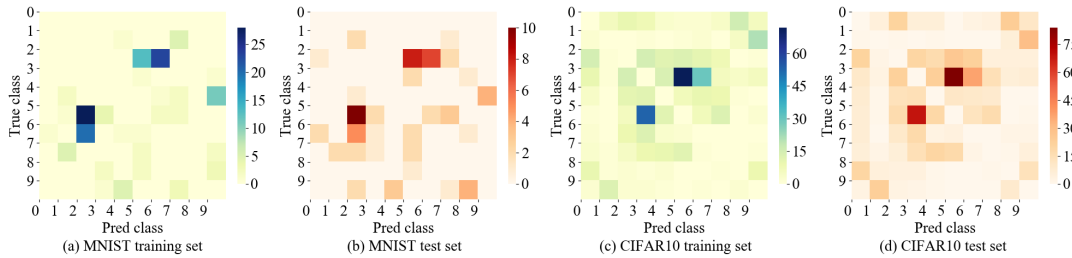


Figure 8: Heatmaps of confusion matrices.

Table 3: Accuracy of original and adversarial trained ResNet32 models on adversarial datasets

Model	MNIST				CIFAR10			
	Adv1 (n=136)	Tr.+Adv1 (n=60k+136)	Adv2 (n=26)	Ts.+Adv2 (n=10k+26)	Adv3 (n=244)	Tr.+Adv3 (n=50k+244)	Adv4 (n=146)	Ts.+Adv4 (n=10k+146)
Original	0.00%	99.53%	0.00%	98.99%	0.00%	98.34%	0.00%	89.97%
Adversarial	83.82%	99.64%	76.92%	99.26%	88.93%	99.05%	63.01%	90.91%

tively, and also up to 76.92% and 63.01% on test-data derived Adv2 and Adv4, respectively. We also observe an increase of 0.27% and 0.94%, respectively, in accuracy on combined data of original test set and its adversarial samples for MNIST and CIFAR10. These results indicate our approach can significantly improve the adversarial defense of DNN classifiers.

4 Conclusion

This paper introduced an FI-and-PSO based framework for adversarial image generation and training for DNN classifiers

by accounting for the user specified number of perturbed pixels, misclassification probability, and/or targeted incorrect class. We used the perturbation-based FI measure to efficiently detect the vulnerable images and pixels to increase the attack success rate. We designed different misclassification loss functions to meet various user's specifications and obtained the optimal perturbation by the fast PSO algorithm. Experiments showed good performance of our approach in generating customized adversarial samples and associated adversarial training for DNNs.

References

Bakas, S.; Reyes, M.; Jakab, A.; Bauer, S.; Rempfler, M.; Crimi, A.; Shinohara, R. T.; Berger, C.; Ha, S. M.; Rozycki, M.; et al. 2018. Identifying the best machine learning algorithms for brain tumor segmentation, progression assessment, and overall survival prediction in the BRATS challenge. *arXiv preprint arXiv:1811.02629* .

Bojarski, M.; Del Testa, D.; Dworakowski, D.; Firner, B.; Flepp, B.; Goyal, P.; Jackel, L. D.; Monfort, M.; Muller, U.; Zhang, J.; Zhang, X.; Zhao, J.; and Zieba, K. 2016. End to end learning for self-driving cars. *arXiv preprint arXiv:1604.07316* .

Carlini, N.; and Wagner, D. 2017. Towards evaluating the robustness of neural networks. In *2017 ieee symposium on security and privacy (sp)*, 39–57. IEEE.

Cook, R. D. 1986. Assessment of local influence. *Journal of the Royal Statistical Society: Series B (Methodological)* 48(2): 133–155.

Eberhart, R.; and Shi, Y. 2001. Particle swarm optimization: developments, applications and resources. In *Proceedings of the 2001 congress on evolutionary computation (IEEE Cat. No. 01TH8546)*, volume 1, 81–86. IEEE.

Goodfellow, I. J.; Shlens, J.; and Szegedy, C. 2014. Explaining and harnessing adversarial examples. *arXiv preprint arXiv:1412.6572* .

He, K.; Zhang, X.; Ren, S.; and Sun, J. 2016. Deep residual learning for image recognition. In *Proceedings of the IEEE conference on computer vision and pattern recognition*, 770–778.

Huang, G.; Liu, Z.; Van Der Maaten, L.; and Weinberger, K. Q. 2017. Densely connected convolutional networks. In *Proceedings of the IEEE conference on computer vision and pattern recognition*, 4700–4708.

Kennedy, J.; and Eberhart, R. 1995. Particle swarm optimization. In *Proceedings of ICNN'95-International Conference on Neural Networks*, volume 4, 1942–1948. IEEE.

Krizhevsky, A. 2009. CIFAR-10 and CIFAR-100 datasets. Available: <https://www.cs.toronto.edu/~kriz/cifar.html> .

Krizhevsky, A.; Sutskever, I.; and Hinton, G. E. 2012. Imagenet classification with deep convolutional neural networks. In *Advances in neural information processing systems*, 1097–1105.

Kurakin, A.; Goodfellow, I.; and Bengio, S. 2016. Adversarial examples in the physical world. *arXiv preprint arXiv:1607.02533* .

LeCun, Y.; Cortes, C.; and Burges, C. 2010. MNIST handwritten digit database. *ATT Labs [Online]*. Available: <http://yann.lecun.com/exdb/mnist> .

Madry, A.; Makelov, A.; Schmidt, L.; Tsipras, D.; and Vladu, A. 2017. Towards deep learning models resistant to adversarial attacks. *arXiv preprint arXiv:1706.06083* .

Meng, D. 2018. Generating deep learning adversarial examples in black-box scenario. *Electronic Design Engineering* 26(24): 164–173.

Meng, D.; and Chen, H. 2017. Magnet: a two-pronged defense against adversarial examples. In *Proceedings of the 2017 ACM SIGSAC Conference on Computer and Communications Security*, 135–147.

Moosavi-Dezfooli, S.-M.; Fawzi, A.; Fawzi, O.; and Frossard, P. 2017. Universal adversarial perturbations. In *Proceedings of the IEEE conference on computer vision and pattern recognition*, 1765–1773.

Moosavi-Dezfooli, S.-M.; Fawzi, A.; and Frossard, P. 2016. Deepfool: a simple and accurate method to fool deep neural networks. In *Proceedings of the IEEE conference on computer vision and pattern recognition*, 2574–2582.

Mosli, R.; Wright, M.; Yuan, B.; and Pan, Y. 2019. They Might NOT Be Giants: Crafting Black-Box Adversarial Examples with Fewer Queries Using Particle Swarm Optimization. *arXiv preprint arXiv:1909.07490* .

Najafabadi, M. M.; Villanustre, F.; Khoshgoftaar, T. M.; Seliya, N.; Wald, R.; and Muharemagic, E. 2015. Deep learning applications and challenges in big data analytics. *Journal of Big Data* 2(1): 1.

Nazemi, A.; and Fieguth, P. 2019. Potential adversarial samples for white-box attacks. *arXiv preprint arXiv:1912.06409* .

Nguyen, A.; Yosinski, J.; and Clune, J. 2015. Deep neural networks are easily fooled: High confidence predictions for unrecognizable images. In *Proceedings of the IEEE conference on computer vision and pattern recognition*, 427–436.

Novak, R.; Bahri, Y.; Abolafia, D. A.; Pennington, J.; and Sohl-Dickstein, J. 2018. Sensitivity and generalization in neural networks: an empirical study. In *International Conference on Learning Representations*. ArXiv preprint arXiv:1802.08760.

Papernot, N.; McDaniel, P.; Jha, S.; Fredrikson, M.; Celik, Z. B.; and Swami, A. 2016. The limitations of deep learning in adversarial settings. In *2016 IEEE European symposium on security and privacy (EuroS&P)*, 372–387. IEEE.

Poli, R. 2008. Analysis of the publications on the applications of particle swarm optimisation. *Journal of Artificial Evolution and Applications* 2008.

Ren, K.; Zheng, T.; Qin, Z.; and Liu, X. 2020. Adversarial Attacks and Defenses in Deep Learning. *Engineering* .

Shu, H.; and Zhu, H. 2019. Sensitivity Analysis of Deep Neural Networks. In *Proceedings of the AAAI Conference on Artificial Intelligence*, volume 33, 4943–4950.

Su, J.; Vargas, D. V.; and Sakurai, K. 2019. One pixel attack for fooling deep neural networks. *IEEE Transactions on Evolutionary Computation* 23(5): 828–841.

Sun, Y.; Liang, D.; Wang, X.; and Tang, X. 2015. Deepid3: Face recognition with very deep neural networks. *arXiv preprint arXiv:1502.00873* .

Szegedy, C.; Zaremba, W.; Sutskever, I.; Bruna, J.; Erhan, D.; Goodfellow, I.; and Fergus, R. 2013. Intriguing properties of neural networks. *arXiv preprint arXiv:1312.6199* .

Wiyatno, R. R.; Xu, A.; Dia, O.; and de Berker, A. 2019. Adversarial Examples in Modern Machine Learning: A Review. *arXiv preprint arXiv:1911.05268* .

Xu, G.; Cui, Q.; Shi, X.; Ge, H.; Zhan, Z.-H.; Lee, H. P.; Liang, Y.; Tai, R.; and Wu, C. 2019. Particle swarm optimization based on dimensional learning strategy. *Swarm and Evolutionary Computation* 45: 33–51.

Zhang, Q.; Wang, K.; Zhang, W.; and Hu, J. 2019. Attacking Black-Box Image Classifiers With Particle Swarm Optimization. *IEEE Access* 7: 158051–158063.

Zhang, Y.; Wang, S.; and Ji, G. 2015. A comprehensive survey on particle swarm optimization algorithm and its applications. *Mathematical Problems in Engineering* 2015.

Zhu, H.; Ibrahim, J. G.; Lee, S.; and Zhang, H. 2007. Perturbation selection and influence measures in local influence analysis. *The Annals of Statistics* 35(6): 2565–2588.

Zhu, H.; Ibrahim, J. G.; and Tang, N. 2011. Bayesian influence analysis: a geometric approach. *Biometrika* 98(2): 307–323.